arXiv:1105.0175v2 [cond-mat.mtrl-sci] 4 May 2011

Quantifying defects in graphene via Raman spectroscopy at different excitation energies

L. G. Cançado[1], A. Jorio[1], E. H. Martins Ferreira[2], F. Stavale[2], C. A. Achete[2], R. B. Capaz[3], M. V. O. Moutinho[3], A. Lombardo[4], T. Kulmala[4], and A. C. Ferrari[4]
[1]*Departamento de Física, Universidade Federal de Minas Gerais, 30123-970, Belo Horizonte, Brazil*
[2]*Divisão de Metrologia de Materiais, Instituto Nacional de Metrologia, Normalização e Qualidade Industrial (INMETRO), Duque de Caxias, RJ 25250-020, Brazil,*
[3]*Instituto de Física, Universidade Federal do Rio de Janeiro, Cx. Postal 68528, Rio de Janeiro, 21941-972 RJ, Brazil, and*
[4]*Department of Engineering, University of Cambridge, Cambridge CB3 0FA, UK.*

We present a Raman study of Ar^+-bombarded graphene samples with increasing ion doses. This allows us to have a controlled, increasing, amount of defects. We find that the ratio between the D and G peak intensities for a given defect density strongly depends on the laser excitation energy. We quantify this effect and present a simple equation for the determination of the point defect density in graphene via Raman spectroscopy for any visible excitation energy. We note that, for all excitations, the D to G intensity ratio reaches a maximum for an inter-defect distance $\sim 3\,$nm. Thus, a given ratio could correspond to two different defect densities, above or below the maximum. The analysis of the G peak width and its dispersion with excitation energy solves this ambiguity.

I. INTRODUCTION

Quantifying defects in graphene related systems, which include a large family of sp^2 carbon structures, is crucial both to gain insight in their fundamental properties, and for applications. In graphene, this is a key step towards the understanding of the limits to its ultimate mobility[1–3]. Large efforts have been devoted to quantify defects and disorder using Raman spectroscopy for nanographites[4–19], amorphous carbons[17–23], carbon nanotubes[24,25], and graphene[11,26–34]. The first attempt was the pioneering work of Tuinstra and Koenig (TK)[4]. They reported the Raman spectrum of graphite and nano-crystalline graphite, and assigned the mode at $\sim$1580 cm^{-1} to the high frequency E_{2g} Raman allowed optical phonon, now known as G peak[5]. In defected and nanocrystalline samples they measured a second peak at $\sim$1350 cm^{-1}, now known as D peak[5]. They assigned it to an A_{1g} breathing mode at the Brillouin Zone (BZ) boundary **K**, activated by the relaxation of the Raman fundamental selection rule $\mathbf{q} \approx \mathbf{0}$, where $\mathbf{q}$ is the phonon wavevector[4]. They noted that the ratio of the D to G intensities varied inversely with the crystallite size, L_a. Ref.[17] noted the failure of the TK relation for high defect densities, and proposed a more complete amorphization trajectory valid to date. Refs.[7,8,17,18] reported a significant excitation energy dependence of the intensity ratio. Refs.[9,10] measured this excitation laser energy dependency in the Raman spectra of nanographites, and the ratio between the D and G bands was shown to depend on the fourth power of the excitation laser energy E_L.

There is, however, a fundamental geometric difference between defects related to the size of a nano-crystallite and point defects in the sp^2 carbon lattices, resulting in a different intensity ratio dependence on the amount of disorder. Basically, the amount of disorder in a nano-crystallite is given by the amount of border (one-dimensional defects) with respect to the total crystallite area, and this is a measure of the nano-crystallite size L_a. In graphene with zero-dimensional point-like defects, the distance between defects, L_D, is a measure of the amount of disorder, and recent experiments show that different approaches must be used to quantify L_D and L_a by Raman spectroscopy[27]. The effect of changing L_D on peak width, frequency, intensity, and integrated area for many Raman peaks in single layer graphene was studied in Ref.[28], and extended to N-layer graphene in Ref.[29], all using a single laser line $E_L = 2.41\,$eV.

Here, to fully accomplish the protocol for quantifying point-like defects in graphene using Raman spectroscopy (or equivalently, L_D), we use different excitation laser lines in ion-bombarded samples and measure the D to G peak intensity ratio. This ratio is denoted in literature as I_D/I_G or I(D)/I(G), while the ratio of their areas, i.e. frequency integrated intensity, as A_D/A_G or A(D)/A(G). In principle, for small disorder or perturbations, one should always consider the area ratio, since the area under each peak represents the probability of the whole process, considering uncertainty[28,35]. However, for large disorder, it is far more informative to decouple the information on peak intensity and full width at half maximum. The latter, denoted in literature as FWHM or Γ, is a measure of structural disorder[10,21,28], while the intensity represents the phonon modes/molecular vibrations involved in the most resonant Raman processes[17,18,21]. For this reason, in this paper we will consider the decoupled I_D/I_G and peak widths trends. We find that, for a given L_D, I_D/I_G increases as the excitation laser energy increases. We present a set of empirical formulas that can be used to quantify the amount of point-like defects in graphene samples with $L_D \geq 10\,$nm using any excitation laser energy/wavelength in the visible range. The analysis of the D and G peak widths and their dispersions with excita-

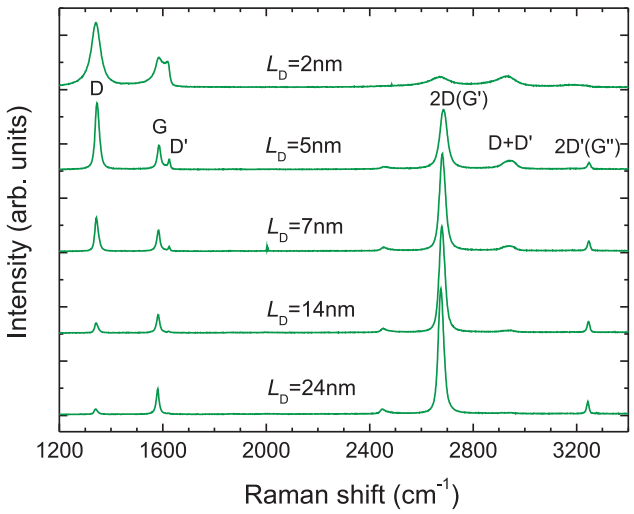

FIG. 1. Raman spectra of five ion bombarded SLG measured at $E_{\rm L}=2.41\,{\rm eV}$ ($\lambda_{\rm L}=514.5\,{\rm nm}$). The $L_{\rm D}$ values are given according to Ref.[27], and the main peaks are labeled. The notation within parenthesis [e.g. 2D(G′)] indicate two commonly used notations for the same peak (2D and G′)[30,40].

tion energy unambiguously discriminate between the two main stages of disordering incurred by such samples.

II. RESULTS AND DISCUSSION

We produce single layer graphene (SLG) samples with increasing defect density by mechanical exfoliation followed by Ar^+-bombardment, as for the procedure outlined in Ref.[27]. The ion-bombardment experiments are carried out in an OMICRON VT-STM ultra-high vacuum system (base pressure $5\times10^{-11}\,{\rm mbar}$) equipped with an ISE 5 Ion Source. Raman spectra are measured at room temperature with a Renishaw microspectrometer. The spot size is $\sim1\,\mu{\rm m}$ for a 100× objective, and the power is kept at $\sim1.0\,{\rm mW}$ to avoid heating. The excitation energies, $E_{\rm L}$, (wavelengths, $\lambda_{\rm L}$) are: Ti-Sapph 1.58 eV (785 nm), He-Ne 1.96 eV (632.8 nm), Ar^+ 2.41 eV (514.5 nm).

Figure 1 plots the Raman spectra of five SLG exposed to different ion bombardment doses in the range 10^{11} Ar^+/cm^2 (one defect per 4×10^4 C atoms) to 10^{15} Ar^+/cm^2 (one defect for every four C atoms). The bombardment procedure described in Ref.[27] is accurately reproducible. By tuning the bombardment exposure we generated samples with $L_{\rm D}=24,14,13,7,5,{\rm and}\,2\,{\rm nm}$. All spectra in Fig. 1 are taken at $E_{\rm L}=2.41\,{\rm eV}$ ($\lambda_{\rm L}=514.5\,{\rm nm}$).

The Raman spectra in Figure 1 consist of a set of distinct peaks. The G and D appear around $1580\,{\rm cm}^{-1}$ and $1350\,{\rm cm}^{-1}$, respectively. The G peak corresponds to the E_{2g} phonon at the Brillouin zone center. The D peak is due to the breathing modes of six-atom rings and requires a defect for its activation[4,17,18,36]. It comes from transverse optical (TO) phonons around the **K** or **K′** points in the 1st Brillouin zone[4,17,18], involves an intervalley double resonance process[36,37], and is strongly dispersive[38] with excitation energy due to a Kohn Anomaly at **K**[39]. Double resonance can also happen as intravalley process, i. e. connecting two points belonging to the same cone around **K** or **K′**[37]. This gives the so-called D′ peak, which is centered at $\sim$ $1620\,{\rm cm}^{-1}$ in defected samples measured at 514.5nm[12]. The 2D peak (also called G′ in the literature) is the second order of the D peak[12,30]. This is a single peak in single layer graphene, whereas it splits in four in bilayer graphene, reflecting the evolution of the electron band structure[30,40]. The 2D′ peak (also called G″ in analogy to G′) is the second order of D′. Since 2D(G′) and 2D′(G″) originate from a process where momentum conservation is satisfied by two phonons with opposite wavevectors, no defects are required for their activation, and are thus always present. On the other hand, the D + D′ band ($\sim2940\,{\rm cm}^{-1}$) is the combination of phonons with different momenta, around **K** and Γ, thus requires a defect for its activation.

Ref.[17] proposed a three stage classification of disorder in carbon materials, to simply assess the Raman spectra of carbons along an amorphization trajectory leading from graphite to tetrahedral amorphous carbon: 1) graphite to nanocrystalline graphite; 2) nanocrystalline graphite to low sp^3 amorphous carbon; 3) low sp^3 amorphous carbon to high sp^3 (tetrahedral) amorphous carbon. In the study of graphene, stages 1 and 2 are the most relevant and are summarized here.

In stage 1, the Raman spectrum evolves as follows[17,27,28]: a) D appears and $I_{\rm D}/I_{\rm G}$ increases; b) D′ appears; c) all peaks broaden. In the case of graphite the D and 2D lose their doublet structure[17,41]; e) D + D′ appears; f) at the end of stage 1, G and D′ are so wide that they start to overlap. If a single lorentzian is used to fit G + D′, this results in an upshifted wide G band at $\sim1600\,{\rm cm}^{-1}$.

In stage 2, the Raman spectrum evolves as follows[17]: a) the G peak position, denoted in literature as Pos(G) or $\omega_{\rm G}$, decreases from $\sim1600\,{\rm cm}^{-1}$ towards $\sim1510\,{\rm cm}^{-1}$; b) the TK relation fails and $I_{\rm D}/I_{\rm G}$ decreases towards 0; c) $\omega_{\rm G}$ becomes dispersive with the excitation laser energy, the dispersion increasing with disorder; d) there are no more well defined second-order peaks, but a small modulated bump from $\sim2300\,{\rm cm}^{-1}$ to $\sim3200\,{\rm cm}^{-1}$[17,28].

In disordered carbons $\omega_{\rm G}$ increases as the excitation wavelength decreases, from IR to UV[17]. The dispersion rate, ${\rm Disp(G)}=\Delta\omega_{\rm G}/\Delta E_{\rm L}$, increases with disorder. The G dispersion separates the materials into two types. In those with only sp^2 rings, Disp(G) saturates at $\sim1600\,{\rm cm}^{-1}$, the G position at the end of stage 1. In contrast, for those containing sp^2 chains (such as in amor-

phous and diamond-like carbons), G continues to rise past $1600\,\mathrm{cm}^{-1}$ and can reach $\sim 1690\,\mathrm{cm}^{-1}$ for 229 nm excitation[17,18]. On the other hand, D always disperses with excitation energy[17,18]. Γ_G always increases with disorder[10,23,27,28]. Thus, combining $I_\mathrm{D}/I_\mathrm{G}$ and Γ_G allows to discriminate between stages 1 or 2, since samples in stage 1 and 2 could have the same $I_\mathrm{D}/I_\mathrm{G}$, but not the same Γ_G, being this much bigger in stage 2[23,27,28].

We note that Figure 1 shows the loss of sharp second order features in the Raman spectrum obtained from the $L_\mathrm{D}=2\,\mathrm{nm}$ SLG. This is an evidence that the range of defect densities in our study covers stage 1 (samples with $L_\mathrm{D}=24, 14, 13, 7, 5\,\mathrm{nm}$) and the onset of stage 2 (sample with $L_\mathrm{D}=2\,\mathrm{nm}$).

Figures 2a-c report the first-order Raman spectra of our ion-bombarded SLGs measured at $E_\mathrm{L}=1.58\,\mathrm{eV}$ ($\lambda_\mathrm{L}=785\,\mathrm{nm}$), 1.96 eV (632.8 nm),2.41 eV (514.5 nm), respectively. Figure 2d shows the Raman spectra of the ion-bombarded SLG with $L_\mathrm{D}=7\,\mathrm{nm}$ obtained using the three different laser energies. We note that $I_\mathrm{D}/I_\mathrm{G}$ considerably changes with the excitation energy. This is a well-know effect in the Raman scattering of sp^2 carbons[9,10,17,18,42,43]. Ref.[10] noted that the integrated areas of different peaks depend differently on excitation energy E_L: while A_D, $A_{\mathrm{D}'}$, and A_2D shown no E_L-dependence, A_G was found to be proportional to E_L^4. The independence of A_2D on E_L agrees with the theoretical prediction[44] if one assumes that the electronic scattering rate is proportional to the energy. However, a fully quantitative theory is not trivial since, in general, A_D depends not only on the concentration of defects, but on their type as well (e.g., only defects able to scatter electrons between the two valleys can contribute)[31,32,34]. Different defects can also produce different frequency and polarization dependence of A_D[31,32,34].

Figure 3 plots $I_\mathrm{D}/I_\mathrm{G}$ for all SLGs and laser energies. For all E_L, $I_\mathrm{D}/I_\mathrm{G}$ increases as L_D decreases (stage 1), reaches a maximum at $L_\mathrm{D}\sim 3\,\mathrm{nm}$, and decreases towards zero for $L_\mathrm{D}<3\,\mathrm{nm}$ (stage 2). It is important to understand what the maximum of $I_\mathrm{D}/I_\mathrm{G}$ vs. L_D means. I_D will keep increasing until the contribution from each defect sums independently[27,31]. In this regime (stage 1) I_D is proportional to the total number of defects probed by the laser spot. For an average defect distance L_D and laser spot size L_L, there are on average $(L_\mathrm{L}/L_\mathrm{D})^2$ defects in the area probed by the laser, thus $I_\mathrm{D}\propto (L_\mathrm{L}/L_\mathrm{D})^2$. On the other hand, I_G is proportional to the total area probed by the laser$\propto L_\mathrm{L}^2$, giving $I_\mathrm{D}/I_\mathrm{G}\propto 1/L_\mathrm{D}^2$[17,27]. However, if two defects are closer than the average distance an e-h pair travels before scattering with a phonon, then their contributions will not sum independently anymore[27,28,31,33]. This distance can be estimated as $v_\mathrm{F}/\omega_\mathrm{D}\sim 3\,\mathrm{nm}$[31], where $v_\mathrm{F}\sim 10^6\,\mathrm{m/s}$ is the Fermi velocity around the $\mathbf{K}$ and $\mathbf{K}'$ points, in excellent agreement with the predictions of Refs.[17] and the data of Refs.[27,28,33]. For an increasing number of defects (stage 2), where $L_\mathrm{D}<3\,\mathrm{nm}$, sp^2 domains become smaller and the rings fewer and more distorted, until they open up. As the G peak is just related to the relative motion of sp^2 carbons, we can assume I_G roughly constant as a function of disorder. Thus, with the loss of sp^2 rings, I_D will decrease with respect to I_G and the $I_\mathrm{D}/I_\mathrm{G}\propto 1/L_\mathrm{D}^2$ relation will no longer hold. In this regime, $I_\mathrm{D}/I_\mathrm{G}\propto M$ (M being the number of ordered rings), and the development of a D peak indicates ordering, exactly the opposite to stage 1[17]. This leads to a new relation: $I_\mathrm{D}/I_\mathrm{G}\propto L_\mathrm{D}^2$[17].

The solid lines in Fig. 3 are fitting curves following the relation proposed in Ref.[27]:

$$\frac{I_\mathrm{D}}{I_\mathrm{G}} = C_\mathrm{A}\frac{(r_\mathrm{A}^2-r_\mathrm{S}^2)}{(r_\mathrm{A}^2-2r_\mathrm{S}^2)}\left[e^{-\pi r_\mathrm{S}^2/L_\mathrm{D}^2}-e^{-\pi(r_\mathrm{A}^2-r_\mathrm{S}^2)/L_\mathrm{D}^2}\right]. \quad (1)$$

The parameters r_A and r_S are length scales which determine the region where the D band scattering takes place. r_S determines the radius of the structurally disordered area caused by the impact of an ion. r_A is defined as the radius of the area surrounding the point defect in which the D band scattering takes place, although the sp^2 hexagonal structure is preserved[27]. In short, the difference $r_\mathrm{A}-r_\mathrm{S}$ defines the Raman relaxation length of the D band scattering, and is associated with the coherence length of electrons which undergo inelastic scattering by optical phonons[27,33]. The fit in Figure 2 is done considering $r_\mathrm{S}=1\,\mathrm{nm}$ (as determined in Ref.[27] and expected to be a structural parameter, i. e. E_L independent). Furthermore, within experimental accuracy, all data can be fit with the same $r_\mathrm{A}=3.1\,\mathrm{nm}$, in excellent agreement with the values obtained in Refs.[27,28,33]. Any uncertainty in r_A does not affect the results in the low defect density regime ($L_\mathrm{D}>10\,\mathrm{nm}$) discussed later.

Ref.[27] suggested that $I_\mathrm{D}/I_\mathrm{G}$ depends on both an activated (A) area, pounded by the parameter C_A, and a structurally defective area (S), pounded by a parameter C_S. Here we selected $C_\mathrm{S}=0$ in eq. (1) for two reasons: (i) C_S should be defect-structure dependent, and in the ideal case where the defect is the break-down of the C-C bonds, C_S should be null; (ii) here we do not focus on the large defect density regime, $L_\mathrm{D}<r_\mathrm{S}$. The parameter C_A in eq. (1) corresponds to the maximum possible $I_\mathrm{D}/I_\mathrm{G}$, which would be observed in the ideal situation where the D band would be activated in the entire sample with no break down of any hexagonal carbon ring[27].

C_A has been addressed in Ref.[27] as related to the ratio between the scattering efficiency of optical graphene phonons evaluated between Γ and $\mathbf{K}$. As we show here, the large $I_\mathrm{D}/I_\mathrm{G}$ dependence on E_L comes from the change on C_A, which suggests this parameter might also depend on interference effects, when summing the different electron/hole scattering processes that are possible when accounting for the Raman cross section[45–49]. Note that C_A decreases as the laser energy increases. The solid line in the inset to Fig. 2 is the fit of the experimental data (dark squares) by using an empirical relation between the maximum value of $I_\mathrm{D}/I_\mathrm{G}$ and E_L, of the form $C_\mathrm{A}=A\,E_\mathrm{L}^{-B}$. The fit yields $A=(160\pm 48)\,\mathrm{eV}^4$, by setting $B=4$ in agreement with Refs.[9,10].

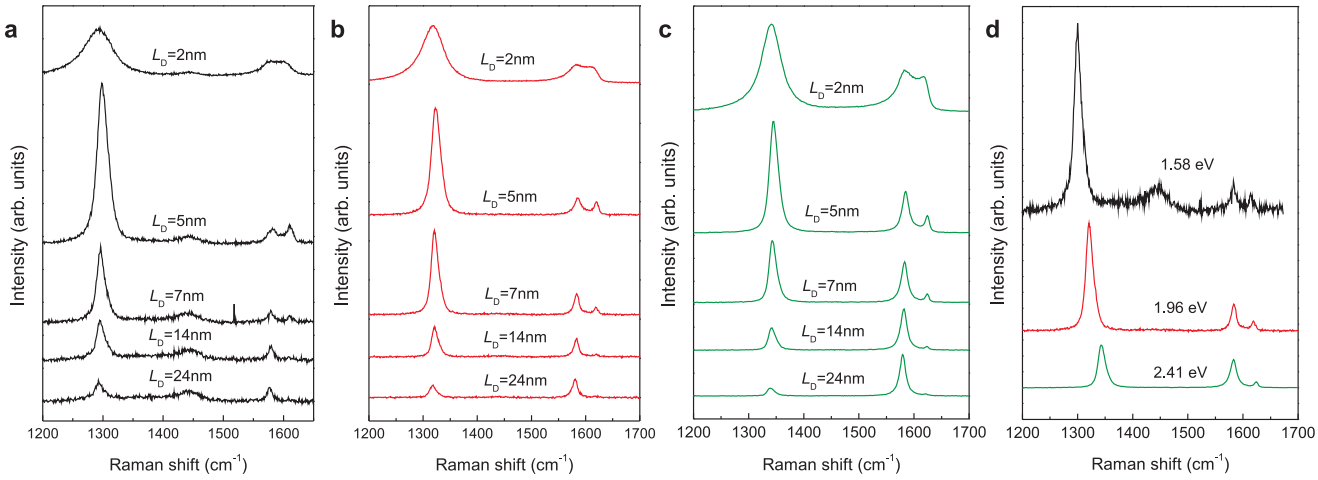

FIG. 2. (a-c) Raman spectra of five distinct ion-bombarded graphene samples using the excitation laser energies (wavelengths) $E_L = 1.58\,\text{eV}$ ($\lambda_L = 785\,\text{nm}$), $E_L = 1.96\,\text{eV}$ ($\lambda_L = 632.8\,\text{nm}$), and $E_L = 2.41\,\text{eV}$ ($\lambda_L = 514.5\,\text{nm}$), respectively. (d) Raman spectra of an ion-bombarded sample with $L_D = 7\,\text{nm}$ obtained using these three excitation laser energies.

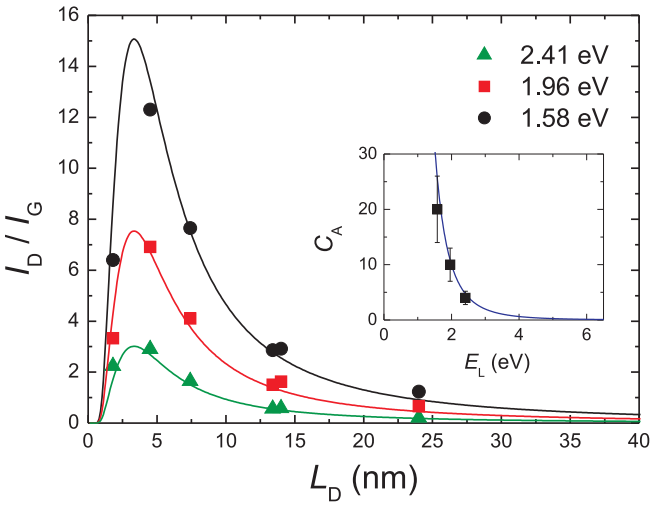

FIG. 3. I_D/I_G for all samples and laser energies considered here. Solid lines are fits according to equation 1 with $r_S = 1\,\text{nm}$, $C_S = 0$, and $r_A = 3.1\,\text{nm}$. The inset plots C_A as a function of E_L. The solid curve is given by $C_A = (160 \pm 48)\,E_L^{-4}$.

We now focus on the low-defect density regime ($L_D \geq 10\,\text{nm}$), since this is the case of most interest in order to understand how Raman active defects limit the ultimate mobility of graphene samples[1–3]. In this regime, where $L_D > 2r_A$, the total area contributing to the D band scattering is proportional to the number of point defects, giving rise to $I_D/I_G \propto 1/L_D^2$, as discussed above. For large values of L_D, eq. (1) can be approximated to

$$\frac{I_D}{I_G} \simeq C_A \frac{\pi(r_A^2 - r_S^2)}{L_D^2}. \qquad (2)$$

By taking $r_A = 3.1\,\text{nm}$, $r_S = 1\,\text{nm}$, and also the relation $C_A = (160 \pm 48)E_L^{-4}$ obtained from the fit of the experimental data shown in Figure 2, eq. (2) can be rewritten as

$$L_D^2\,(\text{nm}^2) = \frac{(4.3 \pm 1.3) \times 10^3}{E_L^4} \left(\frac{I_D}{I_G}\right)^{-1}. \qquad (3)$$

In terms of excitation laser wavelength λ_L (in nanometers), we have

$$L_D^2\,(\text{nm}^2) = (1.8 \pm 0.5) \times 10^{-9} \lambda_L^4 \left(\frac{I_D}{I_G}\right)^{-1}. \qquad (4)$$

Equations (3) and (4) are valid for Raman data obtained from graphene samples with point defects separated by $L_D \geq 10\,\text{nm}$ using excitation lines in the visible range. In terms of defect density $n_D(\text{cm}^{-2}) = 10^{14}/(\pi L_D^2)$, eqs. (3) and (4) become

$$n_D(\text{cm}^{-2}) = (7.3 \pm 2.2) \times 10^9 E_L^4 \left(\frac{I_D}{I_G}\right), \qquad (5)$$

and

$$n_D(\text{cm}^{-2}) = \frac{(1.8 \pm 0.5) \times 10^{22}}{\lambda_L^4} \left(\frac{I_D}{I_G}\right). \qquad (6)$$

Figure 4 plots $E_L^4(I_D/I_G)$ as a function of L_D for the data shown in Figure 2. The data with $L_D > 10\,\text{nm}$ obtained with different laser energies collapse in the same

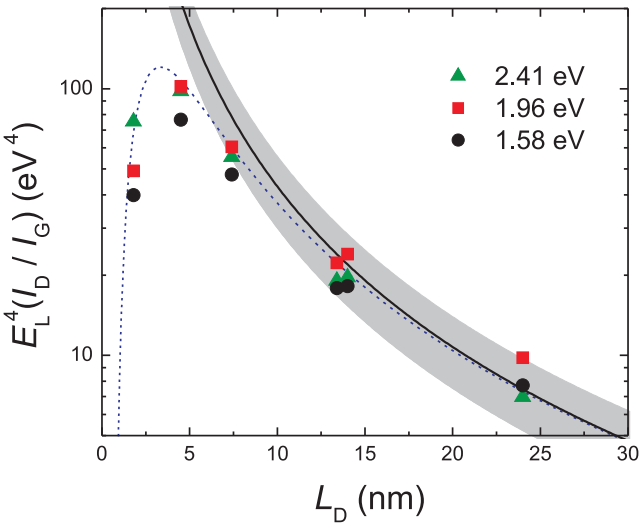

FIG. 4. $E_L^4(I_D/I_G)$ as a function of L_D for the data shown in Figure 2. The dashed blue line is the plot obtained from the substitution of the relation $C_A = (160)/E_L^{-4}$ in equation 1. The solid dark line is the plot of the product $E_L^4(I_D/I_G)$ as a function of L_D according to equation 3. The shadow area accounts for the upper and lower limits given by the ±30% experimental error.

curve. The dashed blue line is the plot obtained from the substitution of the relation $C_A = (160)/E_L^4$ in eq. 1. The solid dark line is the plot $E_L^4(I_D/I_G)$ versus L_D according to eqs. (3) and (4). The shadow area accounts for the upper and lower limits given by the ±30% experimental error. The plot in Fig. 4 validates these relations for samples with $L_D > 10$ nm.

Figure 5a plots Γ_D and Γ_{2D} as a function of L_D. Within the experimental error, a dependence of Γ_D or Γ_{2D} on the excitation energy during stage 1 can not be observed. D and 2D always disperse with excitation energy, with $\Delta\omega_D/\Delta E_L \sim 52\,\mathrm{cm}^{-1}/\mathrm{eV}$, and $\Delta\omega_{2D}/\Delta E_L = 2\Delta\omega_D/\Delta E_L$.

Figures 5b,c plot the G peak dispersion $\mathrm{Disp(G)} = \Delta\omega_G/\Delta E_L$ and $\Gamma_G = \mathrm{FWHM(G)}$ as a function of L_D, respectively. As shown in Figure 5b, $\Delta\omega_G/\Delta E_L$ remains zero until the onset of stage two, when it becomes slightly dispersive ($\Delta\omega_G/\Delta E_L \sim 6\,\mathrm{cm}^{-1}/\mathrm{eV}$). Γ_G (Figure 5c) remains roughly constant at $\sim 14\,\mathrm{cm}^{-1}$, a typical value for as-prepared exfoliated graphene[11,30,50,51], until the onset of stage 2 (corresponding to the maximum I_D/I_G) as suggested in Ref.[23], and shown in Ref.[28] for a single laser line $E_L = 2.41$ eV. Combining I_D/I_G and Γ_G allows to discriminate between stages 1 or 2, since samples in stage 1 and 2 could have the same I_D/I_G, but not the same Γ_G, which is much larger in stage 2[23,28].

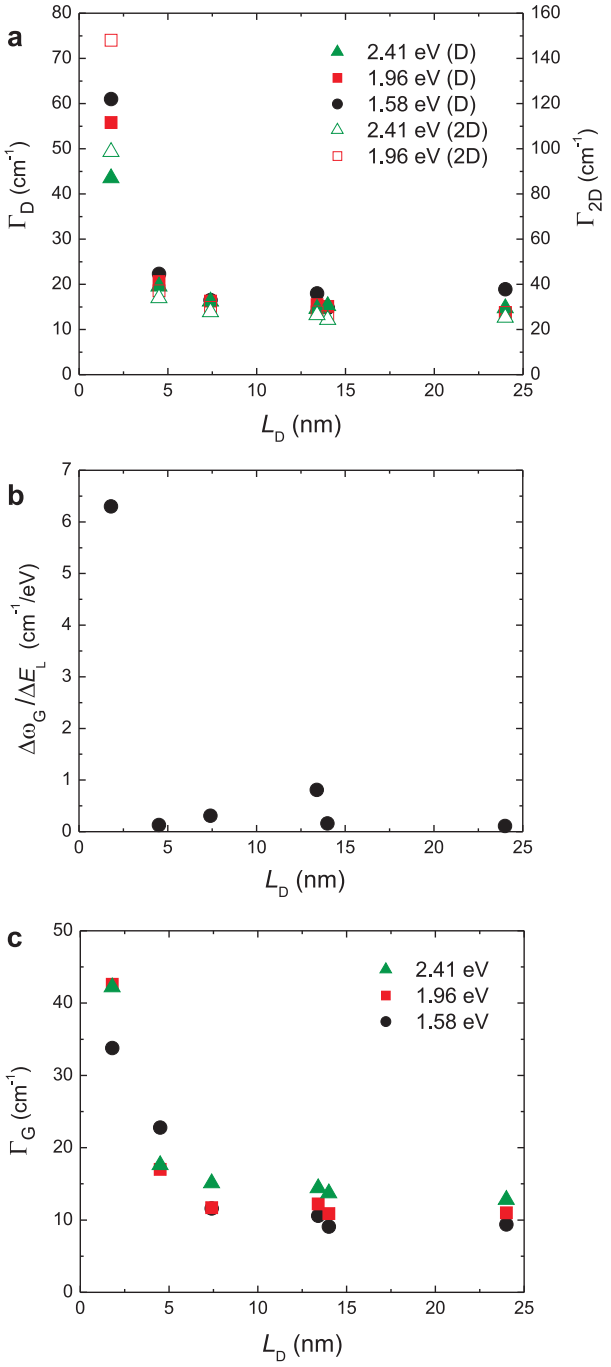

FIG. 5. (a) Plot of Γ_D and Γ_{2D} versus L_D. (b) G peak dispersion [$\mathrm{Disp(G)} = \Delta\omega_G/\Delta E_L$] as a function of L_D. $\Delta\omega_G/\Delta E_L$ remains zero until the onset of stage 2. (c) $\mathrm{FWHM(G)} = \Gamma_G$ as a function of L_D. As suggested in Refs.[23,28], Γ_G remains roughly constant until the onset of the second stage of amorphization, corresponding to the maximum I_D/I_G.

III. CONCLUSIONS

In summary, we discussed the use of Raman spectroscopy for quantifying the amount of point-like defects in graphene. We used different excitation laser lines in ion-bombarded samples in order to measure their respective I_D/I_G. We find that I_D/I_G, for a specific L_D, depends on the laser energy. We presented a set of empirical relations that can be used to quantify point defects in graphene samples with $L_D > 10\,nm$ via Raman spectroscopy using any laser line in the visible range. We show that the Raman coherence length r_A is E_L-independent, while the strong E_L dependence for I_D/I_G comes from the parameter C_A.

IV. ACKNOWLEDGEMENTS

We acknowledge funding from a Royal Society International Project Grant. ACF acknowledges funding from ERC grant NANOPOTS, EPSRC grant EP/G042357/1, a Royal Society Wolfson Research Merit Award, EU grants RODIN and Marie Curie ITN-GENIUS (PITN-GA-2010-264694), and Nokia Research Centre, Cambridge. LGC and AJ acknowledge the support from the Brazilian agencies CNPq and FAPEMIG. EHMF, FS, and CAA acknowledge financial support from Inmetro.

[1] Z. Ni, L. Ponomarenko, R. Nair, R. Yang, S. Anissimova, I. Grigorieva, F. Schedin, P. Blake, Z. Shen, E. Hill, K. S. Novoselov, and A. K. Geim, "On resonant scatterers as a factor limiting carrier mobility in graphene". *Nano Lett.* **10**, 3868-3872 (2010).

[2] J. H. Chen, W. G. Cullen, C. Jang, M. S. Fuhrer, and E. D. Williams, "Defect scattering in graphene". *Phys. Rev. Lett.* **102**, 236805-236808 (2008).

[3] C. R. Dean, A. F. Young, I. Meric, C. Lee, L. Wang, S. Sorgenfrei, K. Watanabe, T. Taniguchi, P. Kim, K. L. Shepard, and J. Hone, "Boron nitride substrates for high-quality graphene electronics". *Nature Nanotech.* **5**, 722-726 (2010).

[4] F. Tuinstra, and J. L. Koenig, "Raman spectrum of graphite". *J. Phys. Chem.* **53**, 1126-1130 (1970).

[5] R. Vidano, and D. B. Fischbach, "New lines in the Raman spectra of carbon and graphite". *J. Am. Ceram. Soc.* **61**, 13-17 (1978).

[6] D. S. Knight, and W. B. White, "Characterization of diamond films by Raman spectroscopy". *J. Mater. Res.* **4**, 385-393 (1989).

[7] K. Sinha, and J. Menendez, "First- and second-order resonant Raman scattering in graphite". *Phys. Rev. B* **41**, 10845-10847 (1990).

[8] M. J. Matthews, M. A. Pimenta, G. Dresselhaus, M. S. Dresselhaus, and M. Endo, "Origin of dispersive effects of the Raman D band in carbon materials". *Phys. Rev. B* **59**, (R)6585-(R)6588 (1999).

[9] L. G. Cançado, K. Takai, T. Enoki, M. Endo, Y. A. Kim, H. Mizusaki, A. Jorio, L. N. Coelho, R. Magalhães-Paniago, and M. A. Pimenta. "General equation for the determination of the crystallite size L_a of nanographite by Raman spectroscopy". *Appl. Phys. Lett.* **88**, 3106-3109 (2006).

[10] L. G. Cançado, A. Jorio, and M. A. Pimenta. "Measuring the absolute Raman cross section of nanographites as a function of laser energy and crystallite size". *Phys. Rev. B* **76**, 064304-064310 (2007).

[11] A. C. Ferrari, "Raman spectroscopy of graphene and graphite: Disorder, electron-phonon coupling, doping and nonadiabatic effects". *Solid State Comm.* **143**, 47-57 (2007).

[12] R. J. Nemanich, S. A. Solim, "First- and second-order Raman scattering from finite-size crystals of graphite". *Phys. Rev. B* **20**, 392-401 (1979).

[13] P. Lespade, A. Marchard, M. Couzi, and F. Cruege, "Caracterisation de materiaux carbones par microspectrometrie Raman". *Carbon* **22**, 375-385 (1984).

[14] A. Cuesta, P. Dhamelincourt, J. Laureyns, A. Martinez-Alonso, J. M. D. Tascon, "Comparative performance of X-ray diffraction and Raman microprobe techniques for the study of carbon materials". *J. Mater. Chem.* **8**, 2875-2879 (1998).

[15] H. Wilhem, M. Lelaurain, E. McRae, and B. Humbert, "Raman spectroscopic studies on well-defined carbonaceous materials of strong two-dimensional character". *J. Appl. Phys.* **84**, 6552-6558 (1998).

[16] M. A. Pimenta, G. Dresselhaus, M. S. Dresselhaus, L. G. Cançado, A. Jorio, and R. Saito, "Studying disorder in graphite-based systems by Raman spectroscopy". *Phys. Chem. Chem. Phys.* **9**, 1276-1291 (2007).

[17] A. C. Ferrari, and J. Robertson, "Interpretation of Raman spectra of disordered and amorphous carbon". *Phys. Rev. B* **61**, 14095-14107 (2000).

[18] A. C. Ferrari, and J. Robertson, "Resonant Raman spectroscopy of disordered, amorphous, and diamondlike carbon". *Phys. Rev. B* **64**, 075414-075426 (2001).

[19] A. C. Ferrari, J. Robertson (Eds.), "Raman spectroscopy in carbons: From nanotubes to diamond". *Philos. Trans. R. Soc. Ser. A* **362**, 2267 (2004).

[20] A. C. Ferrari, and J. Robertson, "Origin of the $1150\,cm^{-1}$ Raman mode in nanocrystalline diamond". *Phys. Rev. B* **63**, (R)121405-(R)121408 (2001).

[21] C. Casiraghi, A. C. Ferrari, and J. Robertson, "Raman spectroscopy of hydrogenated amorphous carbon". *Phys. Rev. B* **72**, 085401-085414 (2005).

[22] B. Racine, A. C. Ferrari, N. A. Morrison, I. Hutchings, W. I. Milne, and J. Robertson, "Properties of amorphous carbon-silicon alloys deposited by a high plasma density source. *J. Appl. Phys.* **90**, 5002-5012 (2001).

[23] A. C. Ferrari, S. E. Rodil, and J. Robertson, "Interpretation of infrared and Raman spectra of amorphous carbon nitrides". *Phys. Rev. B* **67**, 155306-155325 (2003).

[24] M. Hulman, V. Skakalova, S. Roth, and H. J. Kuzmany, "Raman spectroscopy of single-wall carbon nanotubes and graphite irradiated by γ rays". *J. Appl. Phys.* **98**, 024311-024315 (2005).

[25] S. G. Chou, H. Son, J. Kong, A. Jorio, R. Saito, M. Zheng, G. Dresselhaus, and M. S. Dresselhaus, "Length characterization of DNA-wrapped carbon nanotubes using Raman spectroscopy". *Appl. Phys. Lett.* **90**, 131109-131111 (2007).

[26] D. Teweldebrhan, and A. A. Baladin, "Modification of graphene properties due to electron-beam irradiation". *Appl. Phys. Lett.* **94**, 013101-013103 (2009).

[27] M. M. Lucchese, F. Stavale, E. H. Martins Ferriera, C. Vilane, M. V. O. Moutinho, R. B. Capaz, C. A. Achete, and A. Jorio, "Quantifying ion-induced defects and Raman relaxation length in graphene", *Carbon* **48**, 1592-1597 (2010).

[28] E. H. Martins Ferreira, M. V. O. Moutinho, F. Stavale, M. M. Lucchese, R. B. Capaz, C. A. Achete, and A. Jorio, "Evolution of the Raman spectra from single-, few-, and many-layer graphene with increasing disorder". *Phys. Rev. B* **82**, 125429-125437 (2010).

[29] A. Jorio, M. M. Lucchese, F. Stavale, E. H. Martins Ferreira, M. V. O. Moutinho, R. B. Capaz, and C. A. Achete, "Raman study of ion-induced defects in N-layer graphene". *J. Phys.: Condens. Matter* **22**, 334204-334208 (2010).

[30] A. C. Ferrari, J. C. Meyer, V. Scardaci, C. Casiraghi, M. Lazzeri, F. Mauri, S. Piscanec, D. Jiang, K. S. Novoselov, S. Roth, and A. K. Geim, "Raman spectrum of graphene and graphene layers". *Phys. Rev. Lett.* **97**, 187401-187403 (2006).

[31] C. Casiraghi, A. Hartschuh, H. Qian, S. Piscanec, C. Georgi, A. Fasoli, K. S. Novoselov, D. M. Basko, and A. C. Ferrari. "Raman spectroscopy of graphene edges". *Nano Lett.* **9**, 1433-1441 (2009).

[32] B. Krauss, P. Nemes-Incze, V. Skakalova, L. P. Biro, K. von Klitzing, and J. H. Smet, "Raman scattering at pure graphene zigzag edges". *Nano Lett.* **10**, 4544-4548 (2010).

[33] R. Beams, L. G. Cançado, and L. Novotny, "Low temperature Raman study of the electron coherence length near graphene edges". *Nano Lett.* **11**, 1177-1181 (2011).

[34] L. G. Cançado, M. A. Pimenta, B. R. A. Neves, M. S. Dantas, and A. Jorio, "Influence of the atomic structure on the Raman spectra of graphite edges". *Phys. Rev. Lett.* **93**, 247401-247404 (2004).

[35] D. M. Basko, S. Piscanec, and A. C. Ferrari, "Electron-electron interactions and doping dependence of the two-phonon Raman intensity in graphene". *Phys. Rev. B* **80**, 165413-165422 (2009).

[36] C. Thomsen, and S. Reich, "Double resonant Raman scattering in graphite". *Phys. Rev. Lett.* **85**, 5214-5217 (2000).

[37] R. Saito, A. Jorio, A. G. Souza Filho, G. Dresselhaus, M. S. Dresselhaus, and M. A. Pimenta, "Probing phonon dispersion relations of graphite by double resonance Raman scattering". *Phys. Rev. Lett.* **88**, 027401-027404 (2001).

[38] R. P. Vidano, D. B. Fishbach, L. J. Willis, and T. M. Loehr, "Observation of Raman band shifting with excitation wavelength for carbons and graphites". *Solid State Commun.* **39**, 341-344 (1981).

[39] S. Piscanec, M. Lazzeri, F. Mauri, A. C. Ferrari, and J. Robertson, "Kohn anomalies and electron-phonon interactions in graphite". *Phys. Rev. Lett.* **93**, 185503-185506 (2004).

[40] L. G. Cançado, A. Reina, J. Kong, and M. S. Dresselhaus, "Geometrical approach for the study of G′ band in the Raman spectrum of monolayer graphene, bilayer graphene, and bulk graphite". *Phys. Rev. B* **77**, 245408-245416 (2008).

[41] L. G. Cançado, K. Takai, T. Enoki, M. Endo, Y. A. Kim, H. Mizusaki, N. L. Speziali, A. Jorio, and M. A. Pimenta, "Measuring the degree of stacking order in graphite by Raman spectroscopy". *Carbon* **46**, 272-275 (2008).

[42] I. Pocsik, M. Hundhausen, M. Koos, and L. Ley, "Origin of the D peak in the Raman spectrum of microcrystalline graphite". *J. Non-Cryst. Solids* **227-230**, 1083-1086 (1998).

[43] T. P. Mernagh, R. P. Cooney, and R. A. Johnson, "Raman spectra of graphon carbon black". *Carbon* **22**, 39-42 (1984).

[44] D. M. Basko, "Theory of resonant multiphonon Raman scattering in graphene". *Phys. Rev. B* **78**, 125418-125459 (2008).

[45] J. Maultzsch, S. Reich, and C. Thomsen, "Double-resonant Raman scattering in graphite: Interference effects, selection rules, and phonon dispersion". *Phys. Rev. B* **70**, 155403-155411 (2004).

[46] D. M. Basko, "Calculation of the Raman G peak intensity in monolayer graphene: role of Ward identities". *New J. Phys.* **11**, 095011-095022 (2009).

[47] M. Kalbac, A. Reina-Cecco, H. Farhat, J. Kong, L. Kavan, and M. S. Dresselhaus, "The Influence of Strong Electron and Hole Doping on the Raman Intensity of Chemical Vapor-Deposition Graphene". *ACS Nano* **10**, 6055-6063 (2010).

[48] C. F. Chen, C. H. Park, B. W. Boudouris, J. Horng, B. Geng, C. Girit, A. Zettl, M. F. Crommie, R. A. Segalan, S. G. Louie, and F. Wang, "Controlling inelastic light scattering quantum pathways in graphene". *Nature* **471**, 618-620 (2011).

[49] P. Venezuela, M. Lazzeri, and F. Mauri, "Theory of double-resonant Raman spectra in graphene: intensity and line shape of defect-induced and two-phonon bands". arXiv:1103.4582 (2011).

[50] S. Pisana, M. Lazzeri, C. Casiraghi, K. S. Novoselov, A. K. Geim, A. C. Ferrari, and F. Mauri, "Breakdown of the adiabatic Born-Oppenheimer approximation in graphene". *Nature Mat.* **6**, 198-201 (2007).

[51] M. Lazzeri, S. Piscanec, F. Mauri, A. C. Ferrari, and J. Robertson, "Phonon linewidths and electron-phonon coupling in graphite and nanotubes". *Phys. Rev B* **73**, 155426-155431 (2006).